Understanding the Humidity Sensitivity of Sensors with TCAD Simulations

I-S. Ninca[a], I. Bloch[a], B. Brüers[a], V. Fadeyev[b], J. Fernandez-Tejero[c,d], C. Jessiman[e], J. Keller[e], C. T. Klein[e], T. Koffas[e], H. M. Lacker[f], P. Li[f], C. Scharf[f], E. Staats[e], M. Ullan[g], Y. Unno[h]

[a] *DESY Zeuthen, Platanenallee 6, 15738 Zeuthen, Germany ,*
[b] *Santa Cruz Institute for Particle Physics (SCIPP), University of California, Santa Cruz, CA 95064, USA ,*
[c] *Department of Physics, Simon Fraser University, 8888 University Drive, Burnaby, B.C. V5A 1S6, Canada ,*
[d] *TRIUMF, 4004 Wesbrook Mall, Vancouver V6T 2A3, BC, Canada ,*
[e] *Physics Department, Carleton University, 1125 Colonel By Drive, Ottawa, Ontario, K1S 5B6, Canada ,*
[f] *Institut für Physik, Humboldt-Universität zu Berlin, Newtonstraße 15, 12489 Berlin, Germany ,*
[g] *Instituto de Microelectrónica de Barcelona (IMB-CNM), CSIC, Campus UAB-Bellaterra, 08193 Barcelona, Spain ,*
[h] *Institute of Particle and Nuclear Study, High Energy Accelerator Research Organization (KEK), 1-1 Oho, Tsukuba, Ibaraki 305-0801, Japan ,*

Abstract

The breakdown voltage of silicon sensors without special surface is known to be affected by the ambient humidity. To understand the sensor's humidity sensitivity, Synopsys TCAD was used to simulate n-in-p test structures for different effective relative humidity. Photon emission of hot electrons was imaged with a microscope to locate breakdown in the edge-region of the sensor. The Top-Transient Current Technique was used to measure charge transport near the surface in the breakdown region of the sensor. Using the measurements and simulations, the evolution of the electric field, carrier densities and avalanche breakdown in the periphery of p-bulk silicon sensors is presented.

Keywords: ATLAS Experiment, Silicon Sensors, TCAD Simulations, Top-TCT

ATL-ITK-PROC-2024-013
28 February 2024

1. Introduction

The ATLAS ITk will be upgraded to sustain the harsh radiation levels due to the increase in luminosity foreseen at the High-Luminosity Large Hadron Collider (HL-LHC). In the prototyping phase for the new ATLAS ITk Strip detector, silicon sensors showed electrical breakdown at lower bias voltages when exposed to higher humidity [1][1].

The mechanisms that cause the early breakdown of sensors in humid conditions are not yet fully understood. To gain insight into the physical processes that trigger the early avalanche breakdown of sensors due to exposure to humidity, charge transport in the guard-ring region of the test structure was investigated by generating localized free charge carriers near the surface with picosecond pulses of laser light using the Top-Transient Current Technique (TCT). The electrical behavior of test structures was simulated using TCAD from Synopsis [2] and the simulations were crosschecked with the experimental data.

[1] To mitigate this issue the sensors are stored in a dry environment. Once installed, the ITk will be in dry environment and humidity sensitivity will not be an issue during ATLAS operation.

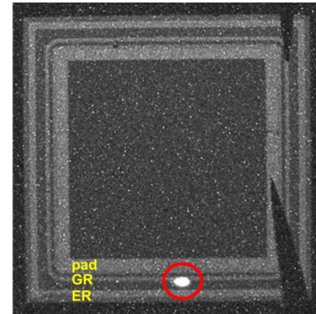

Figure 1: Microscope picture of an n-in-p silicon diode operated in avalanche breakdown. Photon emission from hot electrons in the breakdown region is visible as a bright spot in the bottom of the image. The measurement was performed at an RH of ≈50 %. The breakdown current between the backside and the GR was $\mathcal{O}(1)$ µA.

2. Experimental Methods

2.1. Breakdown imaging

A consumer CMOS camera sensitive in the near infrared spectrum was used to locate avalanche breakdown in the edge region of the test structure. Fig. 1 shows an example $4 \times 4\,\text{mm}^2$ n-in-p diode, biased at -750 V in electrical breakdown. The outermost aluminum ring is called the edge ring (ER), then there is the

guard ring (GR) and finally the pad metal. The bias voltage was applied on backside, which has a conductive coupling to the ER via the undepleted region along the dicing edge. The GR and pad were kept at ground. The bright spot is Bremsstrahlung from hot electrons [3, 4] accelerated in a high electric field between the ER and the GR.

2.2. *Device under test*

For this study, an 8 mm by 8 mm, n-in-p diode called the monitor diode (MD8) was investigated. This type of diode comes from the same ATLAS18 ITk wafer as the strip sensor [5]. The MD8's geometry is similar to the diode illustrated in Fig. 1 but it has a special feature of an additional p-stop between the GR and the pad metal. The active thickness calculated from capacitance-voltage measurements [6] is 295 µm with a full depletion voltage of ≈ -274 V and the effective p-bulk doping is $\approx 4.2 \cdot 10^{12}$cm^{-3}.

2.3. *TCAD geometry implementation*

Structure Device Editor (SDE) was used to implement the MD8 geometry for the TCAD simulations using representative parameters. The cross-section of the test structure is shown in Fig. 2 with a focus on the top edge of the diode. There is a p-implant underneath the ER, while the GR and pad have n-implants. The doping concentration of both the p- and n-implants is 10^{19} cm^{-3}. There is a 0.6 µm SiO_2 layer in direct contact with the silicon that goes beneath the metal overhangs. A 0.6 µm Si_3N_4 layer goes on top of the SiO_2 and the electrodes. The concentration of fixed oxide charges at the interface between the silicon and SiO_2 is $\approx$ 10^{11} cm^{-2} [7]. The values for the parameters implemented are listed in table 1.

Table 1: TCAD Parameters Values

Parameter	Value	Unit
Si p-bulk thickness	295	µm
Si p-bulk doping	$4.2 \cdot 10^{12}$	cm^{-3}
p- and n-implant doping	10^{19}	cm^{-3}
p-stop doping	10^{16}	cm^{-3}
Fixed oxide charge	10^{11}	cm^{-2}
SiO_2/Si_3N_4 thicknesses	0.6	µm

To model the humidity effects on the surface of the test structure, a 0.1 µm polysilicon layer was added on top of the passivation which acts as a resistive layer. It is directly connected to the GR and pad, but it is not in direct contact with the ER since the ER only has passivation openings in the corners of the diode. In the presence of humidity, the sheet resistance $R_\square$ of the passivation surface changes. To simulate a specific RH value, $R_\square$ was adjusted based on literature values [8]. For RH = 40 %, $R_\square$ of the passivation surface of a similar test structure was measured [8] to be $9.7 \cdot 10^{15}$ Ω. To set $R_\square$ of the polysilicon layer in TCAD to this value, the mobility of both electrons and holes in the polysilicon was set to $\mu_{e,h} = 6.7 \cdot 10^{-3}$ cm^2/Vs.

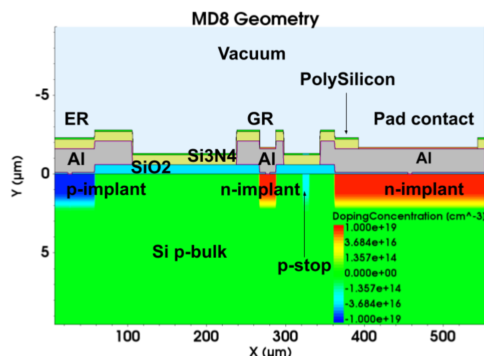

Figure 2: View of the diode geometry used in TCAD. The backside p-implant (not shown) is at Y = 297.2 µm and extends along X.

The carrier mobilities in silicon were described by the Canali model [9] for the high-field saturation and the University of Bologna model [10] for the doping dependence. Shockley–Read–Hall (SRH) recombination with the lifetime $\tau = 10^{-6}$ s and Auger recombination were used. The doping dependence of τ was described using the Scharfetter relation. Charge carrier multiplication was simulated using the van Overstraeten-de Man model [11], which relies on the Chynoweth law [12].

The evolution of the electric field, impact ionization, and the carrier densities over time was simulated as a transient simulation and investigated for several time stamps.

2.4. *Top-TCT*

The Top-TCT method was used to study the charge transport in the region between the ER and the pad of the MD8 diode. Laser pulses of 660 nm wavelength were focused at the sensor's surface with a full width at half maximum of the laser beam $FWHM$ = 7.33 µm±0.16 µm. The laser intensity was 2550 mV corresponding to a few MIPs. The backside was connected to high voltage (HV) and read out via a Bias-T. The ER was also at HV through a conductive channel at the dicing edge to the backside. The GR and pad were

connected to ground[2] as depicted in Fig. 3.

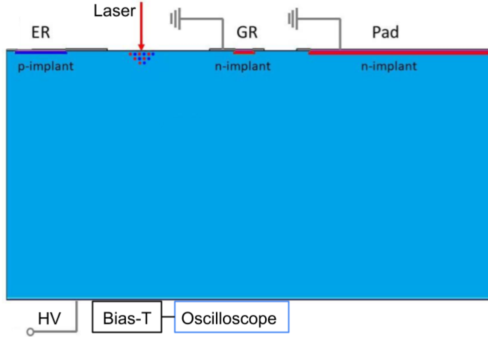

Figure 3: Top-TCT sketch showing electron-hole pair generation by a 660 nm laser pulse between the ER and the GR. During a TCT measurement, the laser beam is moved along the surface of the diode and the induced transients are recorded for each position.

The laser was moved across the diode's surface and the resulting transient current from the drifting charge carriers was recorded at the backside, which has a conductive connection to the edge ring. A Rohde and Schwarz RTO1024 oscilloscope with a sampling rate of 10 Gsample/s and a bandwidth of 2 GHz was used to acquire the current transients averaged over 1000 laser pulses. The humidity inside the TCT set-up was monitored using a humidity sensor placed in the vicinity of the diode. The humidity was controlled by flushing the TCT set-up with dry air until the desired RH value was reached. During the measurements RH was stable within ± 1 %.

Prior to TCT scans, the MD8 diodes were measured in a humidity-controlled probe station. For each RH value, current-voltage (IV) measurements were performed to determine a possible breakdown voltage. However, none of the available MD8 diodes broke down and hot-electron emission could not be recorded for those diodes yet. Previous studies have shown that small structures like mini sensors or diodes show less humidity sensitivity than large ones, such as the ATLAS ITk strip sensors. After each IV is taken, Top-TCT measurements were performed for the exact same RH value. The humidity was ramped up throughout the tests, starting at RH = 10 % to avoid hysteresis effects which can occur when the sensor is biased at high humidity and the humidity is subsequently lowered, freezing a possible charge at the surface [13]. The results shown are from a single diode, MD8 32418-14. For all experimental results, the applied bias voltage was − 1000 V.

[2]Normally, the GR is floating to maximize the breakdown voltage.

The transient current produced by the drift of electrons and holes is given by:

$$I(t) = e_0 \cdot N_{e,h}(t) \cdot \mu_{e,h} \cdot (\vec{E}(\vec{r}(t))) \cdot \vec{E}(\vec{r}(t)) \cdot \vec{E}_w(\vec{r}(t)) \quad (1)$$

where e_0 is the elementary charge, $N_{e,h}(t)$ is the number of electron-hole pairs produced, $\mu_{e,h}(\vec{E}(\vec{r}(t)))$ is the mobility, $\vec{E}(\vec{r}(t))$ is the electric field and $\vec{E}_w(\vec{r}(t))$ is the weighting field.

3. Top-TCT Results

Fig. 4 shows the transient currents for RH= 40 % and multiple positions along a straight line between the ER and the pad metal. It should be noted that the X positions are not aligned and differ in the plots shown in this section. By integrating the transient currents for 43 ns $\leq t \leq$ 80 ns, the total collected charge can be obtained as a function of the laser position, shown in the charge profiles in Fig. 5. Between the ER and GR, the charge profile decreases with increasing the RH. At the same time, the collected charge between the GR and the pad does not change. The high collected charge between the ER and the GR for low humidity is an indication for charge multiplication in the high field at the edge of the GR. In order to test this hypothesis we have measured the collected charge with different laser intensities. The efficiency of charge multiplication strongly depends on the laser intensity [14] as a high concentration of free charge carriers will shield the peak electric field. This can be observed in Fig. 6, where the signal was normalized relative to the values in the pad window. The collected charge near the outer edge of the GR increases with decreasing laser intensity, as expected for charge multiplication in this region.

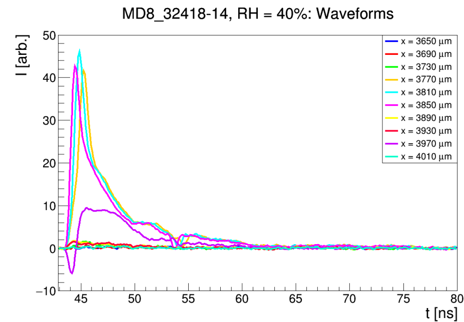

Figure 4: Measured transient currents at different positions in the edge-region of the diode for 40 % RH and $V_{bias} = -1000$ V. The position at $X = 3650$ µm is close to the ER while the position at $X = 4010$ µm is close to the pad. The position of the GR is around $X = 3900$ m.

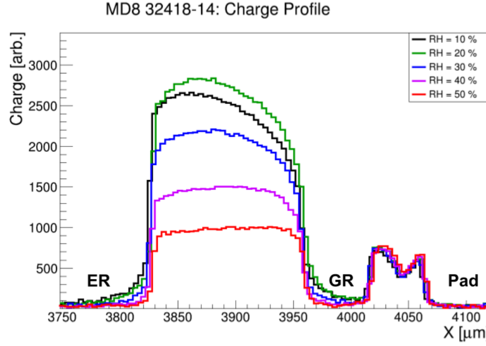

Figure 5: Charge profiles between the ER and pad metalization for different values of RH and $V_{bias} = -1000$ V.

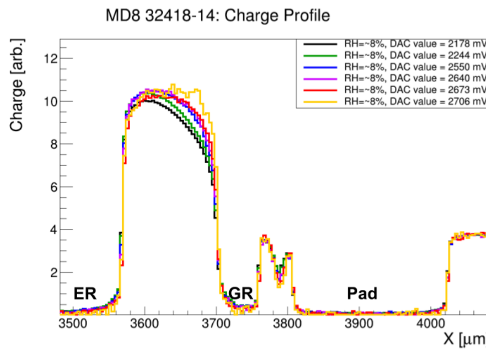

Figure 6: Normalized collected charge between the ER and pad window at RH = 8 %, $V_{bias} = -1000$ V and different laser intensities (a larger DAC value corresponds to a lower intensity). The collected charge was normalized to the charge collected in the pad window, which starts at $X = 4010$ µm, for each laser intensity.

Using a short integration window at the beginning of the current transient, 43,5 ns $\leq t \leq$ 43,9 ns, the prompt current profiles [15] are obtained as shown in Fig.,7. The maximum of the prompt current is near the GR and it decreases as the laser moves away from this electrode. Additionally, the maximum amplitude of the prompt current experiences a decrease with increasing the RH. These observations are an indication that there is a very high electric field (Eq. 1) near the GR and the prompt current in this region might be affected by charge multiplication.

4. TCAD Results

In the TCAD simulation, the bias voltage was ramped from 0 V in steps of 10 V/10 s. After 900 s, the bias voltage was kept constant at − 900 V. All simulations presented here were performed at a RH of 40 %. Fig. 8 shows the simulated reverse current which still increases when the bias voltage is kept constant − 900 V.

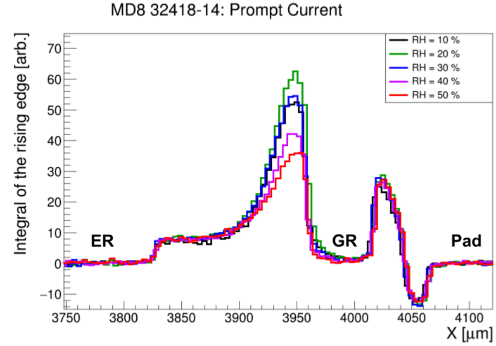

Figure 7: Prompt currents between the ER and pad metalization for different RH and $V_{bias} = -1000$ V.

It is expected that the time constant of this evolution depends strongly on the $R_{\square}$ [13, 8]. Therefore, the simulations were so far only performed for a relatively high RH and cannot be compared to the measurements directly. However, since the measurements were performed first at low RH and the RH was subsequently increased with each measurement, effectively decreasing the time constant, it is expected that the measurements at low RH should be comparable to the simulation right after ramping and the measurements at high RH should be comparable to the simulation after waiting some time at constant bias.

The outcome was analysed in more details at four points in time. The first time stamp, at 900 s, coincides with reaching the final bias voltage of − 900 V. The second time stamp, at 2500 s, was chosen as an intermediate and the third one, at 4500 s, after the leakage current started increasing slowly while the last time stamp, at 6500 s, was chosen after the current started rising rapidly.

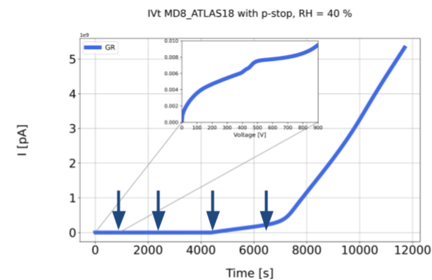

Figure 8: Simulated GR current for RH = 40 % and $V_{const.} = -900$ V for $t > 900$ s. Soft breakdown starts at $t = 4372$ s. The arrows point to the four time stamps chosen to highlight changes in the simulation.

The electrostatic potential for $t = 900$ s is illustrated in Fig. 9. The bias voltage was applied on the back-

side and on the ER, while the GR and the pad were grounded. The biasing scheme is the same as for the Top-TCT measurements.

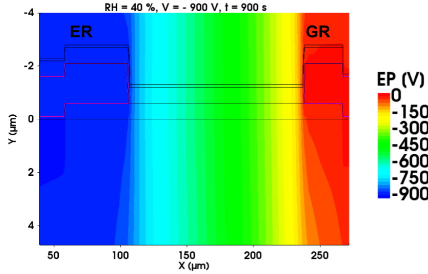

Figure 9: Simulated electrostatic potential for RH = 40 % and V_{bias} = −900 V. The electrostatic potential was extracted immediately after the ramping was finished at t = 900 s.

The absolute electric field shown in Fig. 10 shows a high field peak near the GR which coincides with the location of the maximum measured prompt current in Fig. 7. The TCAD simulation predicts an additional high field peak near the ER which is not visible in the measurement. Once the leakage current starts increasing slowly at t = 4372 s (soft breakdown) the high field at the ER increases. At t = 6500 s, where the leakage current starts rising drastically, new high field regions appear near the ER and GR implants (see Fig. 11). The origin of these maxima and the effect on the breakdown need to be investigated further, but it appears these regions are generating a large amount of free charge carriers by impact ionization.

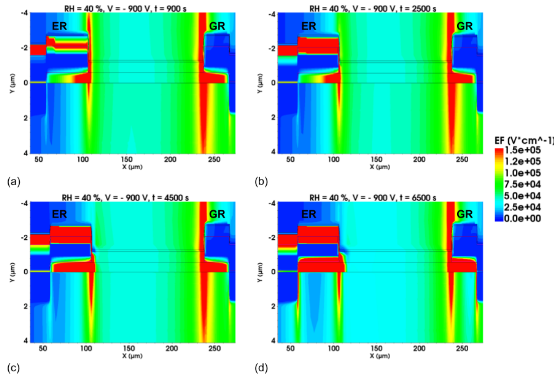

Figure 10: Simulated electric field for RH = 40 %, V_{bias} = −900 V and different time stamps.

The electron density is shown in Fig. 12. Due to the fixed positive oxide charge a conducting electron inversion layer is present at the Si-SiO_2 interface before a bias voltage is applied. The electron inversion layer is

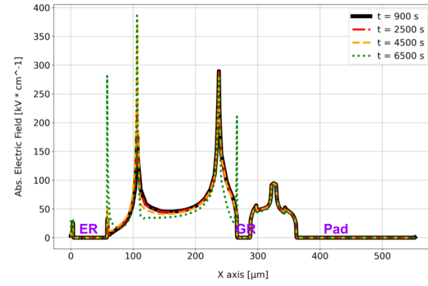

Figure 11: Absolute electric field along X axis 100 nm under the oxide.

dispersed by the electric field when the interface is depleted and the remaining electron concentration at the interface is low after ramping to − 900 V, as seen in Fig. 12a. The increase of the current after some time in humid conditions coincides with an increase of the electron concentration in the inversion layer, as visible in Fig. 12c. It appears that the free electrons generated by impact ionization in the high field region developing at the ER metal edge (see Fig. 10c) replenish the inversion layer. When the current starts to increase rapidly the electron concentration at the interface increases even more (Fig. 12d) and free electrons are also generated at the ER implant.

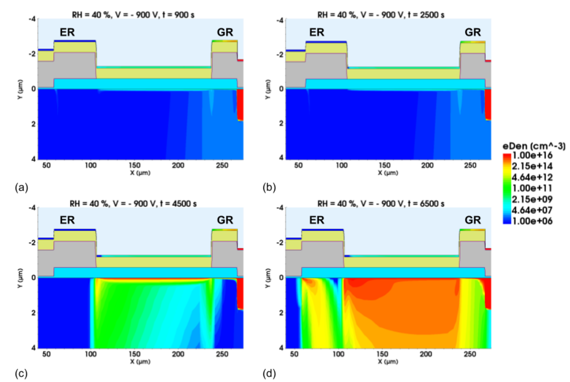

Figure 12: Simulated electron densities for RH = 40 %, V_{bias} = −900 V and different time stamps.

The evolution of the concentration of free holes in the bulk is comparable to the evolution of the electron concentration, as shown in Fig. 13. A high hole concentration is visible near the peaks of the electric field once the current increases. Fig. 13a also shows a high density of holes present in the polysilicon layer on top of the ER after the ramping of the device has finished. It is important to note that the polysilicon layer is capacitively coupled to the ER, while it is in direct electrical contact

with the GR and the pad. Over time, a high concentration of holes in the polysilicon layer moves laterally towards the GR, visible at $X \approx 110\,\mu\text{m}$ in Fig. 13c. It seems to be this positive charging up of the passivation surface that is driving the breakdown. It should be noted that this charging up was not observed in simulations for lower RH, which are not presented here.

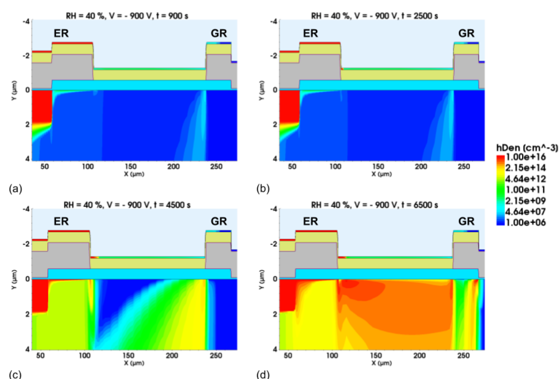

Figure 13: Simulated hole densities for RH = 40 %, $V_{bias} = -900$ V and different time stamps.

Electron-hole pair production due to impact ionization requires a certain electric field strength and is only effective in few regions. After ramping, there is an impact ionisation region underneath the metal overhang of the GR as illustrated in Fig. 14a. At t = 2500 s, Fig. 14b shows a new impact ionization region developing underneath the ER overhang. Following the slow increase of leakage current, the two impact ionization regions start increasing as presented in Fig. 14c. Once the leakage current rises fast, new impact ionization regions develop at the ER and GR implants as highlighted in Fig. 14d.

5. Summary and discussion

Top-TCT measurements and TCAD simulations of silicon sensors with a focus on the guard ring region have been performed at bias values of 900 V and above to study humidity-related breakdown. Electrical breakdown is observed in the TCAD simulation at high humidity after waiting some time at a constant bias voltage. In the sensor used for TCT measurements, no reproducible breakdown stable enough to perform a long term measurement was observed.

The total collected charge in TCT measurements between the guard ring and the edge was observed to decrease with rising relative humidity. The maximum prompt current location observed in the measurement

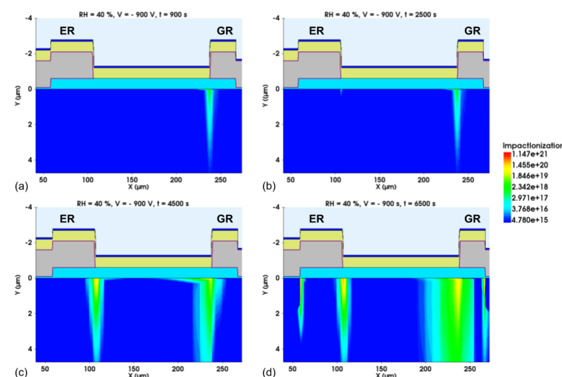

Figure 14: Generation rate of free charge carriers from impact ionization for RH = 40 %, $V_{bias} = -900$ V and different time stamps. For comparison, the bulk generation rate is $U = 4.78 \cdot 10^{15}\,\text{cm}^{-3}\text{s}^{-1}$.

coincides with an electric field peak observed in the TCAD simulation which is sufficiently high to induce charge multiplication of electrons. The signal profile which is observed in the TCT measurement at the edge of the GR at low RH (Fig. 5) can be explained by screening of the charge multiplication [14], also seen in Fig. 6. For high RH less impact ionization is observed at the GR in the measurements. This could be due to less efficient charge multiplications because there are much more free carriers from the electron inversion layer available. The free electrons are generated in a new high field region at the ER in the simulation (Fig. 12c) and drift at the interface into the high field region at the GR, where they can generate more free charge carriers. The development of the new high field region at the ER seems to be caused by a positive charging of the surface of the passivation at the ER. This appears to be a possible cause for humidity-related avalanche breakdown in the guard ring region for the p-bulk sensors at high bias investigated here, assuming the resistive polysilicon layer on the passivation is directly coupled to the GR.

Further measurements in breakdown conditions as well as further simulation studies on the influence of the coupling of the polysilicon layer and the fixed oxide charge density are planned.

Acknowledgments

The work at CNM is part of the Spanish R&D grant PID2021-126327OB-C22, funded by MCIN/ AEI/10.13039/501100011033 / FEDER, UE. The work at SCIPP was supported by the US Department of Energy, grant DE-SC0010107. The work at SFU, TRIUMF and Carleton University was supported by the

Canada Foundation for Innovation and the Natural Sciences and Engineering Research Council of Canada

Declaration of AI and AI-assisted technologies in the writing process

During the preparation of this work the author(s) used ChatGPT 3.5 in order to improve the clarity of the language. After using this tool/service, the author(s) reviewed and edited the content as needed and take(s) full responsibility for the content of the publication.

Copyright

Copyright 2024 CERN for the benefit of the ATLAS Collaboration. Reproduction of this article or parts of it is allowed as specified in the CC-BY-4.0 license.

References

[1] J. Fernandez-Tejero et al., Humidity sensitivity of large area silicon sensors: Study and implications, Nuclear Instruments and Methods in Physics Research Section A: Accelerators, Spectrometers, Detectors and Associated Equipment 978 (2020) 164406.

[2] Synopsys, TCAD - Technology Computer Aided Design, `https://www.synopsys.com/manufacturing/tcad.html`.

[3] N. Akil et al., A multimechanism model for photon generation by silicon junctions in avalanche breakdown, IEEE Transactions on Electron Devices 46 (5) (1999) 1022–1028.

[4] J. Bude et al., Hot-carrier luminescence in Si, Physical Review B 45 (11) (1992) 5848.

[5] Y. Unno et al., Specifications and pre-production of n+-in-p large-format strip sensors fabricated in 6-inch silicon wafers, ATLAS18, for the Inner Tracker of the ATLAS Detector for High-Luminosity Large Hadron Collider, Journal of Instrumentation 18 (03) (2023) T03008.

[6] F. Riemer, Reverse current, capacitance and thermal runaway of irradiated silicon diodes, Master's Thesis, Humboldt-Universität zu Berlin, `https://bib-pubdb1.desy.de/record/471495` (2021).

[7] M. Ullán et al., Quality Assurance methodology for the ATLAS Inner Tracker strip sensor production, Nuclear Instruments and Methods in Physics Research Section A: Accelerators, Spectrometers, Detectors and Associated Equipment 981 (2020) 164521.

[8] D. Brueske et al., Investigation of the insulator layers for segmented silicon sensors before and after X-ray irradiation, in: IEEE Nuclear Science Symposium and Medical Imaging Conference (NSS/MIC), 2014, pp. 1–5. `doi:10.1109/NSSMIC.2014.7431261`.

[9] C. Canali et al., Electron and hole drift velocity measurements in silicon and their empirical relation to electric field and temperature, IEEE Transactions on Electron Devices 22 (11) (1975) 1045–1047.

[10] S. Reggiani et al., Electron and hole mobility in silicon at large operating temperatures. I. Bulk mobility, IEEE Transactions on Electron Devices 49 (3) (2002) 490–499.

[11] R. Van Overstraeten et al., Measurement of the ionization rates in diffused silicon pn junctions, Solid-State Electronics 13 (5) (1970) 583–608.

[12] A. Chynoweth, Ionization rates for electrons and holes in silicon, Physical Review 109 (5) (1958) 1537.

[13] W. Shockley et al., Mobile electric charges on insulating oxides with application to oxide covered silicon pn junctions, Surface Science 2 (1964) 277–287.

[14] E. Currás et al., Gain reduction mechanism observed in low gain avalanche diodes, Nuclear Instruments and Methods in Physics Research Section A: Accelerators, Spectrometers, Detectors and Associated Equipment 1031 (2022) 166530.

[15] G. Kramberger et al., Investigation of irradiated silicon detectors by edge-TCT, IEEE Transactions on Nuclear Science 57 (4) (2010) 2294–2302.